Study of reaction and decay using densities from relativistic mean field theory

G. Gangopadhyay*
Department of Physics, University of Calcutta, Kolkata - 700009, INDIA

Relativistic mean field calculations have been performed to obtain nuclear density profile. Microscopic interactions have been folded with the calculated densities of finite nuclei to obtain a semi-microscopic potential. Life time values for the emission of proton, alpha particles and complex clusters have been calculated in the WKB approach assuming a tunneling process through the potential barrier. Elastic scattering cross sections have been estimated for proton-nucleus scattering in light neutron rich nuclei. Low energy proton reactions have been studied and their astrophysical implications have been discussed. The success of the semi-microscopic potentials obtained in the folding model with RMF densities in explaining nuclear decays and reactions has been emphasized.

I. INTRODUCTION

Relativistic mean field (RMF) approach has proved to be very successful in explaining different features of stable and exotic nuclei such as ground state binding energy, deformation, radius, excited states, spin-orbit splitting, neutron halo, etc[1]. Particularly, the radius and the nuclear density are known to be well reproduced in this model. In nuclei far away from the stability valley, the single particle level structure undergoes certain changes in which the spin-orbit splitting plays an important role. Being based on the Dirac Lagrangian density, and thus naturally incorporating the spin degree of freedom, RMF is particularly suited to investigate these nuclei.

RMF calculations have been found to provide good description of densities, particularly at large radii. Processes, such as proton and alpha decay, low energy scattering and reaction, probe this part of the nuclear volume. Thus, a good description of such processes may be expected if we use microscopic nucleon-nucleon (NN) interactions and densities from RMF calculations to construct nucleon(nucleus)-nucleus potentials. This will be very useful to extend any calculation to areas far from the stability valley, where data are scarce and difficult to obtain in near future. For example, low energy reactions are very important from the astrophysical point of view. In astrophysical environments, neutron and proton reactions are the keys to nucleosynthesis of heavy elements. However, very often, the target nuclei are not available in terrestrial laboratories and one needs to depend on theoretical inputs.

The presentation has been arranged in the following manner. In Section 2, the method of constructing the potential is outlined. The next section presents a few theoretical results for density, followed by selected results of calculation for decays involving emission of proton, alpha and complex clusters. We also briefly discuss the results of elastic proton scattering in neutron rich nuclei. A few low energy proton reactions in $A = 60 - 80$ region have also been studied and astrophysical importance of such reactions has been discussed, Finally, we summarize our results.

II. METHOD

There is a large body of work for the topics that have been presented in this talk. In this section, we restrict ourselves to the salient points of the method of calculation that have been followed to obtain the semi-microscopic potentials used in the present work.

Theoretical density profiles have been ex-

*Electronic address: ggphy@caluniv.ac.in

tracted from RMF calculations. In this approach, nucleons interact via exchange of a number of mesons. There are different variations of the Lagrangian density as well as a number of different parametrizations. In the present work we have employed the FSU Gold[2] Lagrangian density. It contains, apart from the usual component describing a system of nucleons interacting via exchange of mesons, nonlinear terms involving self coupling of the scalar-isoscalar and the vector-isoscalar meson, as well as coupling between the vector-isoscalar meson and the vector-isovector meson.

In the conventional RMF+BCS approach for even-even nuclei, the Euler-Lagrange equations are solved under the assumptions of classical meson fields, time reversal symmetry, no-sea contribution, etc. Pairing is introduced under the BCS approximation. Since accuracy of the nuclear density is very important in our calculation, we have solved the equations in co-ordinate space. The strength of the zero range pairing force is taken as 300 MeV-fm for both protons and neutrons. These values have been chosen to represent a good fit for the binding energy values. In nuclei containing odd number of neutrons or protons, the tagging approximation has been used to specify the level occupied by the last odd nucleon of either type. We have observed that moderate variations of the pairing strength do not influence the results to any great extent.

Effective NN interactions, such as density dependent M3Y (DDM3Y)[3–5], or that of Jeukenne, Lejeune and Mahaux (JLM)[6] may be used to construct the nucleon (nucleus)-nucleus potential. Both the interactions mentioned above have been derived from nuclear matter calculation and have been applied in finite nuclei with success.

The DDM3Y interaction[3, 4] is obtained from a finite range energy independent M3Y interaction by adding a zero range energy dependent pseudopotential and introducing a density dependent factor. The density dependence may be chosen as exponential[3] or be of the form $C(1-\beta\rho^{2/3})$[4]. The constants were obtained from nuclear matter calculation[5] as $C = 2.07$ and $\beta = 1.624$ fm^2. We have adopted all the standard parameters in our calculation without any modification. This interaction has been employed widely in the study of nucleon nucleus as well as nucleus nucleus scattering and radioactivity.

In the JLM potential[6], finite range of the interaction has been introduced by including a Gaussian form factor[7]. Here, we have adopted the global parameters for the interaction and the default normalizations[7].

The semi-microscopic nuclear potentials have been obtained by folding the interactions with the microscopic densities obtained in the RMF calculation. The Coulomb potential has similarly been obtained by folding the Coulomb interaction with the microscopic proton densities. The spin-orbit potential was chosen from the Scheerbaum prescription[8]. The total potential consists of the nuclear part, the Coulomb potential as well as the centrifugal potential. We have not included the contribution of isovector (Lane) potential. However, we expect its effect to be small.

III. RESULTS

A. Density

The charge density has been obtained from the point proton density ρ_p by convoluting with a Gaussian form factor to account the finite size of the proton. We plot in Fig. 1 the calculated charge density for ^{62}Ni and ^{66}Zn as representatives of our results. One can see that the theoretical and experimental values agree very well, particularly at larger radii values, which is the region expected to contribute to the optical potential at low energy. Other nuclei also show similar agreement.

B. Decay

Life time values have been calculated for different types of decays, *i.e.* proton, alpha and cluster radioactivity. We employ the super-asymmetric fission model (SAFM). The decay

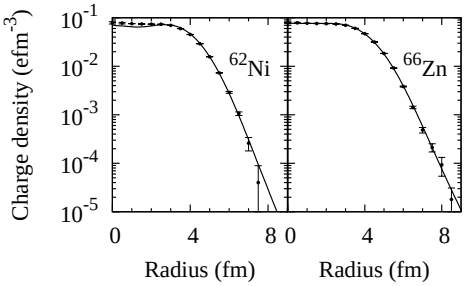

FIG. 1: Calculated charge density in ^{62}Ni and ^{66}Zn (solid lines) compared with experimental measurements (filled circles).

product is assumed to tunnel through the barrier created by the repulsive Coulomb (and the centrifugal) potential and attractive nuclear potential, constructed by folding. The probability of barrier penetration has been calculated in the WKB approximation. The assault frequency is obtained from the zero-point vibration energy[9] that, in turn, has been calculated from the Q-values. Unlike some other works, we have not normalized the optical potential, and have used the values that were obtained from nuclear matter calculations, for the decay studies.

Many calculations exist for proton radioactivity[10]. Our results for the proton radioactivity half life calculation, in nuclei where such decay has been observed from low energy states, are tabulated in Table I. For comparison, we have also presented the results for the DDM3Y interaction of Basu et al.[11], who have used a simple phenomenological form of the densities. We have also shown the uncertainties in the calculated half life values corresponding to the errors in the measured Q-values within parentheses. Our results deviate from experimental measurements in ^{147}Tm, ^{150}Lu and ^{156}Ta, and more prominently in ^{185}Bi and ^{177}Tl*, the last two results being off by an order of magnitude. One can show that the last two discrepancies can be explained as the effect of configuration mixing[10].

It was often suggested that the half life values for proton radioactivity of ^{109}I and ^{112,113}Cs could not be reproduced without the inclusion of deformation effects. For example, a deformation of the order of $\beta \sim 0.05 - 0.15$ was judged to be essential to explain the observed data. However, our calculation reproduces the data for ^{109}I with considerable accuracy. In the deformed calculations, it is usually assumed that the deformation of the parent and the daughter nuclei are identical. The daughter in this particular case is ^{108}Te. Te nuclei are well known vibrational nuclei with very small deformation. One possibility may be that the deficiency of the Woods Saxon potential far away from the stability valley was

TABLE I: Proton decay half lives (T) for spherical proton emitters with even neutron number. Results are for the DDM3Y interaction. The angular momentum of the proton involved is given by l.

Nucleus	l	$\log_{10}$T(s)		
	($\hbar$)	Exp.	Present	Ref[11]
^{105}Sb	2	$2.049^{+0.058}_{-0.067}$	2.27(46)	1.97(46)
^{109}I	2	$-3.987^{+0.020}_{-0.022}$	−4.03(4)	−4.25
^{113}Cs	2	$-4.777^{+0.018}_{-0.019}$	−5.34(4)	−5.53
^{145}Tm	5	$-5.4097^{+0.109}_{-0.146}$	−5.20(6)	−5.14(6)
^{147}Tm	5	$0.591^{+0.125}_{-0.175}$	0.98(4)	0.98(4)
^{147}Tm*	2	$-3.444^{+0.046}_{-0.051}$	−3.26(6)	−3.39(5)
^{151}Lu	5	$-0.896^{+0.011}_{-0.012}$	−0.65(3)	−0.67(3)
^{151}Lu*	2	$-4.796^{+0.026}_{-0.027}$	−4.72(10)	−4.88(9)
^{155}Ta	5	$-4.921^{+0.125}_{-0.125}$	−4.67(6)	−4.65(6)
^{157}Ta	0	$-0.523^{+0.135}_{-0.198}$	−0.21(11)	−0.43(11)
^{161}Re	0	$-3.432^{+0.045}_{-0.049}$	−3.28(7)	−3.46(7)
^{161}Re*	5	$-0.488^{+0.056}_{-0.065}$	−0.57(7)	−0.60(7)
^{165}Ir*	5	$-3.469^{+0.082}_{-0.100}$	−3.52(5)	−3.51(5)
^{171}Au	0	$-4.770^{+0.185}_{-0.151}$	−4.84(15)	−5.02(15)
^{171}Au*	5	$-2.654^{+0.054}_{-0.060}$	−3.03(4)	−3.03(4)
^{177}Tl	0	$-1.174^{+0.191}_{-0.349}$	−1.17(25)	−1.36(25)
^{177}Tl*	5	$-3.347^{+0.095}_{-0.122}$	−4.52(5)	−4.49(6)
^{185}Bi	0	$-4.229^{+0.068}_{-0.081}$	−5.33(13)	−5.44(13)
^{112}Cs	2	$-3.301^{+0.079}_{-0.097}$	−2.93(11)	−3.13
^{150}Lu	5	$-1.180^{+0.055}_{-0.064}$	−0.59(4)	−0.58(4)
^{150}Lu*	2	$-4.523^{+0.620}_{-0.301}$	−4.24(15)	−4.38(15)
^{156}Ta	2	$-0.620^{+0.082}_{-0.101}$	−0.22(7)	−0.38(7)
^{156}Ta*	5	$0.949^{+0.100}_{-0.129}$	1.66(10)	1.66(10)
^{160}Re	2	$-3.046^{+0.075}_{-0.056}$	−2.86(6)	−3.00(6)
^{164}Ir	5	$-3.959^{+0.190}_{-0.139}$	−3.95(5)	−3.92(5)
^{166}Ir	2	$-0.824^{+0.166}_{-0.273}$	−0.96(10)	−1.11(10)
^{166}Ir*	5	$-0.076^{+0.125}_{-0.176}$	0.22(8)	0.21(8)

responsible for the failure of the earlier calculations. We also stress that our results are nearly identical for both the NN interactions. The results for ^{113}Cs and to some extent ^{112}Cs are not reproduced so well, which may be an effect of deformation. However, in none of them do we have an order of magnitude disagreement between theory and experiment as obtained in certain other calculations.

Alpha decay have been studied in Refs. [12–14]. For emission of complex products, there is another factor, the spectroscopic factor, introduced to incorporate the preformation probability. It contains the nuclear structure effects, and may be thought as the overlap between the actual ground state configuration of the parent and the configuration described by the complex decay product coupled to the ground state of the daughter. Obviously, it is expected to be much less than unity as there are contributions from many other configurations other than the one mentioned above.

In a small mass region, we do not expect the spectroscopic factor to vary to any large extent. For example, in the superheavy nuclei presented in Fig. 2, we have taken a constant value 1.4×10^{-2} for all the decays from a fit of the half life values[12]. In some other calculations, the spectroscopic factors have been calculated from theory or phenomenological formulas have been obtained for them[13].

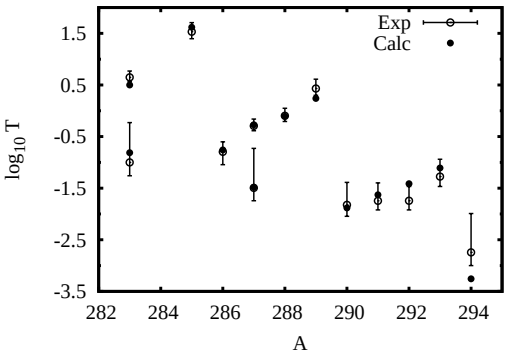

FIG. 2: Calculated and experimental half life values in superheavy nuclei

The above method may be extended to study emission of complex clusters [15, 16]. Basu [17] has studied the nuclear cluster radioactivity also in the framework of SAFM using a phenomenological density and the realistic M3Y interaction. Bhagwat and Gambhir [15] have used densities from RMF calculations. It has been suggested[18] that in the case of decay of heavy clusters, the spectroscopic factor may scale as

$$S = (S_\alpha)^{(A-1)/3} \tag{1}$$

where A is the mass of the heavy cluster and S_α is the spectroscopic factor for the α-decay. Thus a plot of $\log_{10} S$ against A should be a straight line. In Fig. 3, we have plotted the negative of $\log_{10} S$ for the decays where both the parent and the daughter are even-even nuclei against the mass number of the cluster and plotted a best fit line. One can see that the points fall nearly on a straight line.

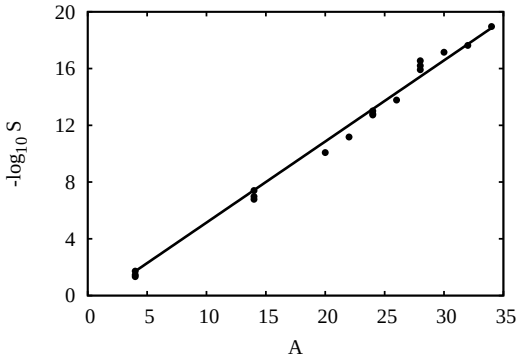

FIG. 3: Negative of logarithm of spectroscopic factors (S) as a function of cluster mass number A for even-even parents and daughters.

C. Elastic scattering

Elastic proton scattering in inverse kinematics provides a test for the calculated densities, particularly in absence of electron scattering data. Density information is not available in exotic neutron rich nuclei in very light

mass region. Elastic scattering cross sections for scattering of these nuclei from proton target have been calculated[19] with the optical model potential generated in the semi-microscopic approach. In Fig. 4, the measured partial cross sections for proton scattering of ^{6,8}He in inverse kinematics have been compared with theory. The real and the imaginary parts of the potential have been chosen as 0.8 times and 0.2 times the folded value for the DDM3Y potential. One can see that the experimental values are nicely reproduced.

D. Low energy proton reactions of astrophysical significance

Capture and charge exchange reactions at very low energy play a very important role in nucleosynthesis. Particularly, rapid proton capture (rp) process in explosive nucleosynthesis is a basic ingredient in driving the abundance along the $N = Z$ line[20]. As this process has to overcome a large Coulomb barrier, it can occur only at a higher temperature range. For example, X-ray bursts provide large fluxes of protons at peak temperatures around 1-2 GK and are expected to play a significant role in the creation of nuclei up to mass 110.

The rp-process proceeds along the $N = Z$ line in mass 60-80 region. In nature, the important proton capture reactions may involve certain nuclei as targets which are not available to us. Hence, experimental information is difficult, if not impossible, to obtain, at least in near future. In such a situation, one has to rely on theory for the reaction rates. Cross sections were calculated for proton capture reactions in mass 60-80 region using semi-microscopic optical potentials in the local density approximation with phenomenological density prescriptions. However, far from the stability valley, these prescriptions may not represent the actual densities very well, leading to considerable uncertainties in the reaction rates. Very often, the reactions rates are varied by a large factor to study their effects. For example, Schatz[21] varied the rates of certain reactions by a factor of one hundred. Obviously, this makes the results uncertain to some extent and affects the final abundance.

A fully microscopic calculation may be used to estimate the rates to reduce the above uncertainty. A consistent framework for calculation may be constructed based on microscopic densities and may be extended to unknown mass regions with confidence. In the present work, we have tried to calculate the reaction rates taking densities from a purely microscopic model, *i.e.* RMF. We have already mentioned that RMF is particularly suitable to describe nuclei far away from the stability valley where experimental knowledge is scarce. A semi-microscopic optical potential obtained by folding an appropriate microscopic NN interaction is expected to be more accurate and may do away with the necessity of any arbitrary variation in the reaction rates.

However, even in a semi-microscopic optical potential, there often remain certain parameters that can be fixed only after comparison with experiment. We have compared the results for a number of (p, γ) and (p, n) reactions in mass region $A = 60 - 80$ for which experimental cross sections are available. This has helped us in determining a set of parameters for this mass region.

The reaction calculations have been performed with the computer code TALYS 1.2[22] assuming spherical symmetry for the target nuclei. The real part of the potential has been obtained by normalizing the folded DDM3Y potential by a factor of 0.7, while the imaginary part, by a factor of 0.1, so as to explain the S-factors obtained in the above experiments. We have employed the full Hauser-Feshbach calculation with transmission coefficients averaged over total angular momentum values and with corrections due to width fluctuations. The gamma ray strength has been calculated in the HFB and HF+BCS model.

In Figs. 5 and 6, we plot the results of our calculations for S-factors and compare them with experimental values for (p, γ) reactions for various targets in mass 60-70 region. The energy relevant to the rp-process in this mass

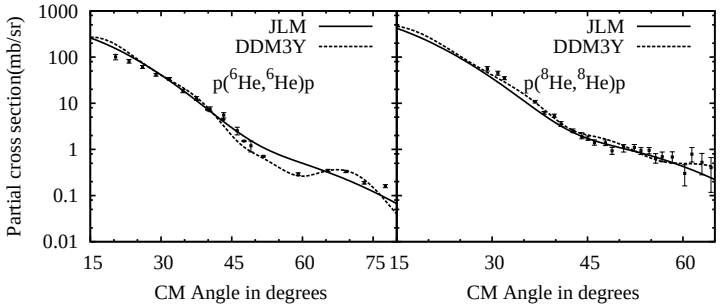

FIG. 4: Partial cross section for elastic proton scattering in inverse kinematics. The projectile energies of ^{6}He and ^{8}He are 71 MeV/A and 72 MeV/A, respectively.

region lies between 1.1 to 3.5 MeV. As the cross-section varies very rapidly at such low energy, a comparison between theory and experiment is rather difficult. The usual practice in low energy nuclear reaction is to compare another key observable, *viz.* the S-factor. It is given by

$$S(E) = E\sigma(E)e^{2\pi\eta} \tag{2}$$

where E is the energy in centre of mass frame in keV, $\sigma(E)$ indicates reaction cross-section in barn and η is the Sommerfeld parameter with

$$2\pi\eta = 31.29 Z_p Z_t \sqrt{\frac{\mu}{E}} \tag{3}$$

Here, Z_p and Z_t are the charge numbers of the projectile and the target, respectively and μ is the reduced mass (in amu). The quantity S-factor varies much more slowly than reaction cross-sections as the exponential energy dependence of cross-section is not present in it. For this reason, we calculate this quantity and compare it with experimentally extracted values.

In Fig. 7, we plot the results for cross sections to populate the ground state and the first two excited states for ^{63,65}Cu(p,γ) reactions. Results for proton capture by other nuclei as well as charge exchange reactions have also been calculated in this mass region and found to agree reasonably well with experimental observations[23–27].

Once the parameters have been fixed, we employ them to calculate the rates of a number of astrophysically important proton reactions. Some very important $N = Z$ nuclei, which have the highest abundance in an equilibrium in a chain, are termed as waiting points[20] for the chain. These nuclei have negative or small positive Q-values for proton capture. An equilibrium between the $(p,\gamma)/(\gamma,p)$ processes is established and the *rp* process may have to wait for beta-decay or α-capture to proceed to heavier nuclei. Certain $N = Z$ waiting point nuclei with $A < 80$, *viz.* ^{64}Zn, ^{68}Se, ^{72}Kr, and ^{76}Sr have long half lives, their total lifetime being large compared to the time scale of typical X-ray bursts (10-100 sec). Thus, they may produce a bottleneck in the *rp*-process that would slow down the rate of hydrogen burning and necessitate extended burst tails unless two proton capture can reduce these half lives and bridge the waiting points. X-ray burst model calculations are therefore particularly sensitive to the rates of proton capture for these nuclei. We have used the microscopic approach, outlined in the present work, to calculate the rates with an aim to study the bridging of the waiting point nuclei.

For calculation of proton capture at waiting points, a small network, which includes the following processes, has been employed. The waiting point nucleus with $Z = N$, which acts as a seed, may capture a proton. The re-

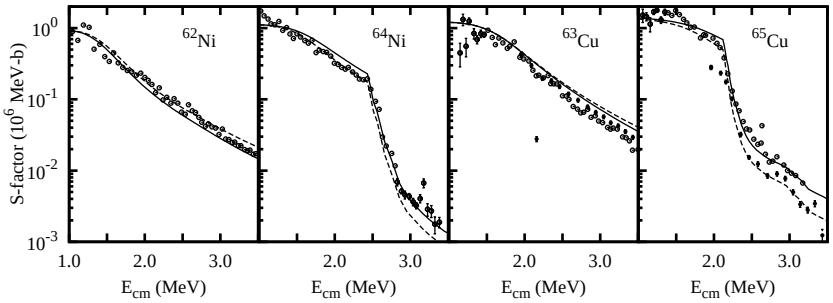

FIG. 5: S-factors extracted from experimental measurements compared with theory for ^{62,64}Ni and ^{63,65}Cu targets. Solid and dashed lines indicate respectively the results of the HF+BCS and HFB approaches for level density and E1 gamma strength.

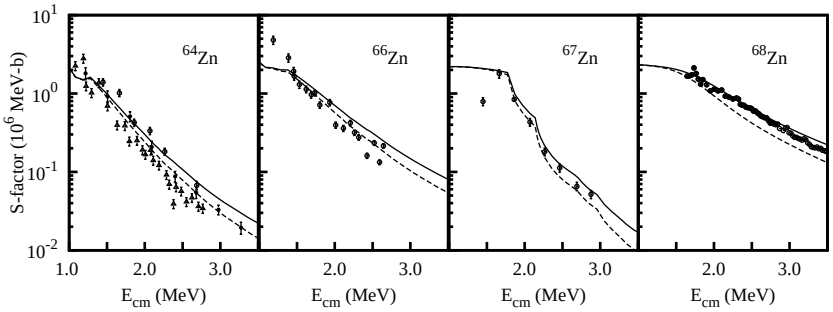

FIG. 6: S-factors extracted from experimental measurements compared with theory for $^{64,66-68}$Zn. See caption of Fig. 5 for details.

sulting nucleus, with $Z = N + 1$, may either capture another proton or undergo photodisintegration emitting a proton to go back to the seed nucleus. The nucleus with $Z = N+2$ may also undergo photodisintegration. In addition, all the three nuclei mentioned above may undergo β-decay. The photodisintegration rates at different temperatures have been calculated from the proton capture rates using the principle of detailed balance. The density has been taken as 10^6 gm/cm^3 unless otherwise mentioned. The proton fraction has been assumed to be 0.7.

Fig. 8 shows the change in the effective half life of ^{64}Ge in explosive hydrogen rich environment. For comparison, we have also plotted the results calculated from the rates in Rauscher et al.[28] by dash-dotted lines. The effects of the uncertainties on the half life values in the Q-values have been indicated in the figures by dotted lines. The half life decreases and possibly goes to a value substantially less than ten seconds, the minimum duration of an X-ray burst. However, one sees that the uncertainty in mass measurement prevents one from reaching any firm conclusion. Depending on the actual value of the masses, it may even be possible that a burst of the order of ten seconds cannot bridge this waiting point effectively.

A larger network, starting from ^{56}Ni seed and consisting of (p, γ), (γ, p) reactions and β-decay, has been employed to study the the time evolution of abundance. In Fig. 9 we plot

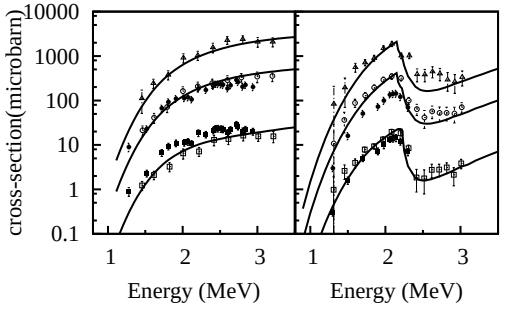

FIG. 7: Partial cross sections for (p,γ) reactions to the low-lying states in Zn for ^{63}Cu (left panel) and ^{65}Cu (right panel) targets. Squares, circles and triangles represent data for transition to the ground state, the first excited state (multiplied by 10) and the second excited state (multiplied by 100), respectively.

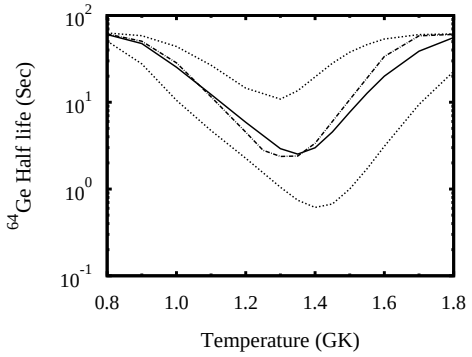

FIG. 8: Effective half life values of ^{64}Ge as a function of temperature. The solid line represents the results of our calculation while the dotted lines mark the two extremes for the errors in the Q-values of the reactions involved. The dash dotted line shows the results obtained using the rates from [28].

the path followed by the *rp*-process between $A = 56$ and $A = 80$ for $T = 1.2$ GK. The dark boxes indicate the waiting point nuclei. The elements are indicated at the left of the diagram while the neutron numbers are shown at the bottom. The lines indicate the path followed by nucleosynthesis. The paths through which more than 10% of the total flux flows are

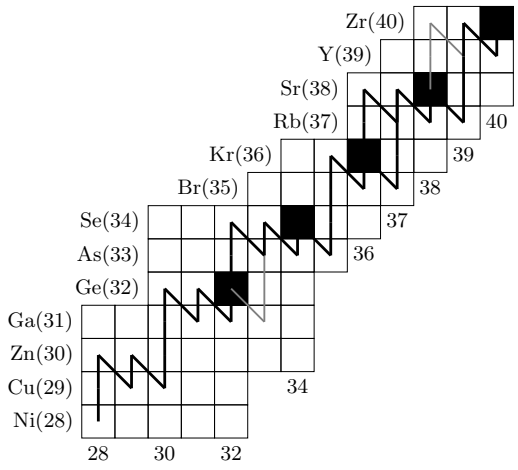

FIG. 9: The rp-process path for 1.2 GK.

indicated by black lines while gray lines show the corresponding paths for flux between 1% - 10%. One can see that ^{64}Ge is easily bridged by two proton capture at 1.2 GK. However, we have found that at a higher temperature, *viz.* 1.5 GK, this waiting point delays the process so that the β-decay of ^{64}Ge contributes significantly. At the next waiting point, ^{68}Se, the photodisintegration is sufficiently strong so that, independent of the temperature, β-decay is practically the only available path. This delays the nucleosynthesis significantly. At ^{72}Kr, the inverse process predominates in higher temperature driving the flux through β-decay. Thus, here also, lower temperature helps nucleosynthesis speed up. The waiting point at ^{76}Sr presents a different picture where the path essentially does not depend on the temperature and principally flows along decay. It is clear that the actual process is significantly dependent on the model of the burst process where the temperature and the proton fraction are functions of time.

The abundance at two different temperatures are plotted as a function of time in Fig. 10. We find that at 1.2 GK, at the end of 100 seconds, the population that reaches $A = 80$ or beyond is more than 1.5 times than the corresponding quantity at the higher temperature of 1.5 GK. In both the cases, the popu-

lation beyond $A = 76$ is significant. It should be noted that these numbers are strongly dependent on the masses of the nuclei near the waiting point. Masses of these nuclei have either not been measured, or measured very imprecisely. Thus one has to depend on theory. In fact, the final abundance at various masses change by a large factor as one uses estimates from different formulas. This conclusion is in agreement with the variation in effective half life values seen in Fig. 8. In the present instance, the Duflo-Zuker formula[29] has been used.

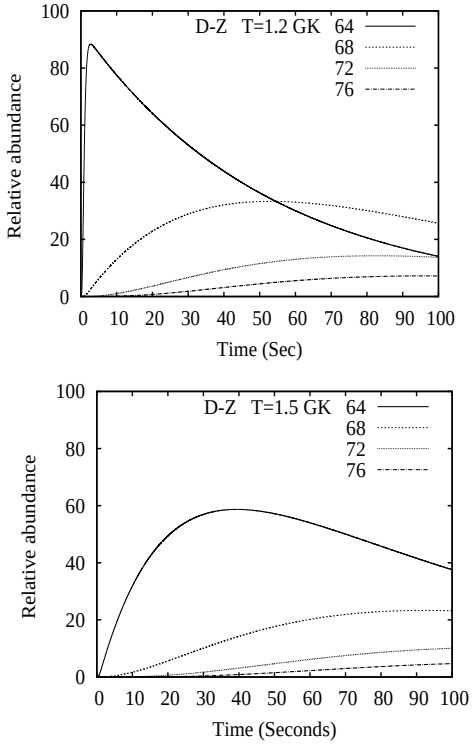

FIG. 10: Evolution of abundance of mass at the waiting points in explosive proton-rich astrophysical environments.

IV. SUMMARY

The techniques used to obtain semi-microscopic optical potentials from theoretical densities using RMF and effective NN interactions have been described. Life time for emission of protons, neutrons and complex nuclei from nuclei have been successfully calculated in the WKB approximation using the real part of the above potential. The potential has also been used to describe elastic scattering and proton reactions at low energy. Astrophysical implications of the results of proton capture reactions have been discussed. Representative results for above calculations have been presented. It is possible to conclude that semi-microscopic optical potentials obtained in the folding model with RMF densities are very much successful in explaining nuclear decays and reactions over the entire mass region.

Acknowledgments

The work presented is actually a joint effort with contributions from Madhubrata Bhattacharya, Chirashree Lahiri, Partha Roy Chowdhury, Abhijit Bhattacharyya and Subinit Roy. Financial assistances provided by the DAE-BRNS and the UGC sponsored DRS Programme of the Department of Physics of the University of Calcutta are gratefully acknowledged.

References

[1] See *e.g.* P. Ring, Prog. Part. Nucl. Phys **37**, 193 (1996).
[2] J. Piekarewicz and B.G. Todd-Rutel, Phys. Rev. Lett. **95**, 122501 (2005).
[3] A. M. Kobos, B. A. Brown, R. Lindsay and G. R. Satchler, Nucl. Phys. **A425**, 205 (1984).
[4] A. K. Chaudhuri, Nucl. Phys. **A449**, 243 (1986); **A459**, 417 (1986).
[5] D.N. Basu, J. Phys. G: Nucl. Part. Phys. **30**, B7 (2004).
[6] J.P. Jeukenne, A. Lejeune and C. Mahaux, Phys. Rev. C **14**, 1391 (1974).
[7] E. Bauge, J.P. Delaroche and M. Girod, Phys. Rev. C **63**, 024607 (2001).

[8] R.R. Scheerbaum, Nucl. Phys. **A257**, 77 (1976).
[9] Y. K. Gambhir, A. Bhagwat, and M. Gupta, Phys. Rev. C **71**, 037301 (2005).
[10] M. Bhattacharya and G. Gangopadhyay, Phys. Lett. B **651**, 263 (2007).
[11] D. N. Basu, P. Roy Chowdhury and C. Samanta, Phys. Rev. C **72**, 051601(R) (2005); P. Roy Chowdhury, C. Samanta and D. N. Basu, Arxiv nucl-th 0511090 (2005).
[12] M. Bhattacharya and G. Gangopadhyay, Phys. Rev. C **77**, 047302 (2008).
[13] G. Gangopadhyay, J. Phys. G: Nucl. Part. Phys. **36**, 095105 (2009); M. Bhattacharya, S. Roy and G. Gangopadhyay, Phys. Lett. **B 665**, 182 (2008).
[14] P. Roy Chowdhury, G. Gangopadhyay and A. Bhattacharyya, Phys. Rev. C **83**, 027601 (2011).
[15] A. Bhagwat and Y.K. Gambhir, Phys. Rev. C**71**, 017301 (2005).
[16] M. Bhattacharya and G. Gangopadhyay, Phys. Rev. C **77**, 027603 (2008).
[17] D. N. Basu, Phys. Rev. C **66**, 027601 (2002).
[18] R. Blendowske and H. Walliser, Phys. Rev. Lett. **61**, 1930 (1988).
[19] G. Gangopadhyay and Subinit Roy, J. Phys. G: Nucl. Part. Phys. **31**, 1111 (2005); M. Bhattacharya, G. Gangopadhyay and Subinit Roy, communicated (2011).
[20] C. Illiadis, *Nuclear Physics of the Stars* (Wiley-VCH Verlag GmbH, Weinheim, 2007).
[21] H. Schatz, Int. J. Mass Spec. **251**, 293 (2006).
[22] A.J. Koning et al., Proc. Int. Conf. Nucl. Data Science Tech., April 22-27, 2007, Nice, France, EDP Sciences, (2008) p. 211.
[23] A. Bhagwat and Y.K. Gambhir, J. Phys. G: Nucl. Part. Phys. **30**, B13 (2004).
[24] G. Gangopadhyay, Phys. Rev. C **82**, 027603 (2010).
[25] C. Lahiri and G. Gangopadhyay, Eur. Phys. J. A **47**, 87 (2011).
[26] C. Lahiri and G. Gangopadhyay, to appear in Phys. Rev. C (2011).
[27] C. Lahiri and G. Gangopadhyay, to appear in Int. J. Mod. Phys. E (2011).
[28] T. Rauscher and F.K. Thielemann, At. Data Nucl. Data Tables **75**, 1 (2000).
[29] J. Duflo and A.P. Zuker, Phys. Rev. C**52**, R23 (1995); Phys. Rev. C**59**, R2347 (1999).